HAL
open science

Photoionization cross sections of iron isonuclear sequence ions: Fe2+ to Fe6+

N. El Hassan, J. M. Bizau, Christophe Blancard, Philippe Cossé, D. Cubaynes, Gérald Faussurier, F. Folkmann

To cite this version:

N. El Hassan, J. M. Bizau, Christophe Blancard, Philippe Cossé, D. Cubaynes, et al.. Photoionization cross sections of iron isonuclear sequence ions: Fe2+ to Fe6+. Physical Review A, 2009, 79, pp.33415. 10.1103/PhysRevA.79.033415 . hal-03733005

HAL Id: hal-03733005

https://hal.science/hal-03733005v1

Submitted on 29 Jul 2022

HAL is a multi-disciplinary open access archive for the deposit and dissemination of scientific research documents, whether they are published or not. The documents may come from teaching and research institutions in France or abroad, or from public or private research centers.

L'archive ouverte pluridisciplinaire **HAL**, est destinée au dépôt et à la diffusion de documents scientifiques de niveau recherche, publiés ou non, émanant des établissements d'enseignement et de recherche français ou étrangers, des laboratoires publics ou privés.

Photoionization cross sections of iron isonuclear sequence ions: Fe^{2+} to Fe^{6+}

N. El Hassan,[1] J. M. Bizau,[1] C. Blancard,[2,3] P. Cossé,[2] D. Cubaynes,[1] G. Faussurier,[2] and F. Folkmann[4]
[1]*Laboratoire d'Interaction des Rayons X avec la Matière (LIXAM), UMR 8624 du CNRS, Université Paris-Sud, B. 350, 91405 Orsay Cedex, France*
[2]*CEA/DAM/DIF, F-91297 Arpajon, France*
[3]*LUTH, Observatoire de Paris, CNRS, Université Paris-Diderot, 5 Place Jules Janssen, 92190 Meudon, France*
[4]*Department of Physics and Astronomy, University of Aarhus, DK-8000 Aarhus C, Denmark*
(Received 19 December 2008; published 24 March 2009)

We have measured the absolute photoionization cross sections of Fe^{2+} to Fe^{6+} ions in the photon energy range covering the first ionization threshold up to 160 eV. Particular interest is emphasized on the region of the $3p \rightarrow 3d$ excitations. The experimental data are compared to the results of calculations we have performed using a spectral opacity code, as well as to available *R*-matrix and one-electron calculations. It is shown that often the theoretical results tend to overestimate the intensity of the $3p \rightarrow 3d$ photoexcitations. An anomalously low value of the integrated oscillator strength is measured for Fe^{2+} ion.

DOI: 10.1103/PhysRevA.79.033415 PACS number(s): 32.80.Fb, 32.80.Zb

I. INTRODUCTION

This paper presents our experimental and theoretical determinations of the photoionization cross sections into the *M* shell of the first ions of the iron isonuclear sequence. Because iron is the heaviest element synthesized during the regular life of the stars, it presents a relatively high cosmic abundance and plays a particular role in astrophysics. Most of the astronomical objects exhibit spectral features of iron ions in various charge state depending on the plasma temperature [1]. Fe ions are, therefore, of great diagnostic values over a broad spectral range, from infrared to hard x-rays. For example, the determination of the chemical composition of ionized plasmas, which present a particularly strong contribution of low ionization states of iron, can be deduced from the observation of the Fe ion photoabsorption lines if their excitation energy and oscillator strength are precisely known [2,3]. Iron ions are also the principal contributors to energy transfer inside the stellar shells. Photoabsorption, which is the main process for energy deposition, reaches its maximum intensity in the extreme ultraviolet (xuv) spectral range (a few tens of eV to 1 keV) [4,5]. The same process is responsible, in fusion research, for cooling of the plasmas—iron acting like an impurity [6]. The determination of plasma opacity requires, in particular, the accurate knowledge of photoionization cross sections.

Several experimental approaches have been developed to study the spectral properties of iron ions, individually or in plasmas. One consists in the measurement of the photoabsorption spectrum of plasmas. For example, the dynamic hohlraum x-ray source at the Sandia National Laboratories Z facility has been used to measure the transmission of a mixed Mg-Fe plasma heated to 156 ± 6 eV at a density of $n_e = 6.9 \pm 1.7 \times 10^{21}$ cm^{-3} [7]. Laser-induced fluorescence, among other techniques, was used also at the Lund Laser Centre to determine reliable oscillator strengths for spectral lines of singly-ionized iron group elements (FERRUM Project) [8]. An alternative approach, allowing to determine absolute photoionization cross sections for mass- and charge-selected ions, uses the merged-beam technique [9,10]. Concerning iron ions, only results for singly [11] and four times charged [12] ions have been published up to now, both obtained at the ASTRID Danish synchrotron-radiation facility in Aarhus University.

All these techniques share the difficulty to produce sufficient density ionic targets. This is particularly true for metallic iron due to the high temperature needed for its vaporization. This explains why experimental results on the photoionization processes on metallic ions are still scarce. Most of the photoionization parameters are known from theoretical investigations [9,10]. In particular, extensive databases of photoionization cross sections on ionic species are available from calculations performed using various atomic models, from the simplest central field approximation [13–15] to the sophisticated *R*-matrix model. The last one was used first in the frame of the Opacity Project [16] and Iron Project [17]. Then, it has been improved by including relativistic effects using the Breit-Pauli approximation, and it has been used to calculate inner-shell excitations [18].

Together with the transition elements, the low charge states of iron ions represent one of the most complex systems regarding fundamental atomic physics. The large number of allowed states arising from the open $3d$ subshell results in very complex atomic systems that are extremely difficult to describe due to the strong influence of electron correlations. The situation is further complicated in the region of the $3p \rightarrow 3d$ "giant resonance" by the addition of one hole in the $3p$-inner subshell, producing numerous resonance lines overlapping due to their large natural width, the so-called unresolved transition arrays (UTAs). Many studies have already focused on the behavior of $3p \rightarrow 3d$ transitions, in particular along $3d$ metal atoms [19] and singly-charged ion [20] sequences.

In the following, we will present the results of our measurements on the photoionization processes on the Fe^{2+} to Fe^{6+} ions obtained using the merged-beam technique at the ASTRID storage ring. The photon energy region we have investigated covers the first ionization threshold of each charge state up to 160 eV, including the region of the $3p \rightarrow 3d$ excitations. We have performed calculations using a code developed for the determination of the spectral opacity

 ©2009 The American Physical Society

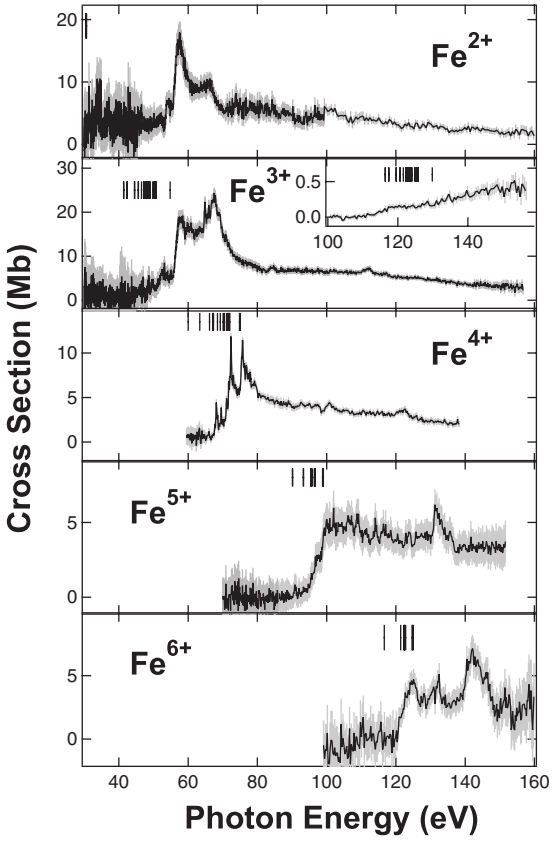

FIG. 1. Variation in the experimental photoionization cross sections, from top to bottom, of Fe^{2+} to Fe^{6+} ions as a function of photon energy. The zones in gray represent the statistical uncertainty. The ionization thresholds for ions in the levels with the same configuration as the ground state are shown as vertical bars [24]. The inset in the second panel from the top displays the double photoionization cross section for Fe^{3+} ion.

of hot plasmas (OPAS). The experimental cross sections will be compared to the results of this code, as well as the results of previously published central field and *R*-matrix calculations.

II. EXPERIMENTAL DETAILS AND RESULTS

The measurements were performed using the same setup as in our previous experiments on Fe^{4+} ions [12]. Here, we will give only a short description of the setup and experimental procedure. More extensive details could be found in Ref. [21]. In short, iron ions are produced within an electron cyclotron resonance ion source (ECRIS) with the help of the resistively heated standard micro-oven developed at the Gesellschaft für Schwerionenforschung (GSI) in Darmstadt [22]. The oven is introduced into the plasma chamber, and a temperature of about 1300 °C is needed to obtain a vapor pressure of the order of 10^{-3} mbar in the chamber. After extraction of the Fe^{Q+} ions from the source by application of a 6 kV extraction voltage followed by deceleration to $2Q$ keV kinetic energy, the ions are selected using a dipole magnet. Typical ion-beam currents in the interaction region were of the order of 10 nA. The photoionization cross sections are obtained by merging the selected ion beam with the monochromatized photon beam emitted from the ASTRID undulator and measuring the resulting $Fe^{(Q+n)+}$ ion yield as a function of photon energy with $n=1$. In the case of the Fe^{3+} ion, we have measured also the $n=2$ double-ionization process. The $Fe^{(Q+n)+}$ ions are separated from the Fe^{Q+} parent ion beam using a second dipole magnet and are counted with a Johnston multiplier. All the parameters needed to extract absolute cross sections are recorded simultaneously, including the spatial overlap between the photon and ion beams and the absolute photon flux [21]. To compensate for the low density of the ionic targets, the spectra were recorded with rather large exit slit widths on the monochromator, especially in the high-energy region where no strong resonance lines are expected. It results in relatively high photon bandpasses, whose calculated values are summarized in Table I for the various energy regions explored for each ion state [21]. The spectral resolutions increase smoothly with the photon energy inside the limits given in the table. Below the 50 eV photon energy, an aluminum filter was inserted in the photon beam to suppress the contribution of higher-order radiation diffracted by the grating. Typical counting rates recorded at the photon energy of the larger resonance with the chopper open and close, respectively, are 12 and 1 Hz for Fe^{2+}, 20 and 6 Hz for Fe^{3+}, 20 and 13 Hz for Fe^{4+}, 6 and 3 Hz for Fe^{5+}, and 16 and 10 Hz for Fe^{6+}.

TABLE I. Lower and upper limits of the photon bandpasses used in different photon energy regions to measure the cross section for the various ion states.

	Energy region (eV)	Bandpass range (eV)
Fe^{2+}	30–60	0.10–0.87
	60–100	0.24–0.87
	100–160	1.67–4.98
Fe^{3+}	30–45	0.06–0.25
	45–65	0.13–0.43
	65–100	0.30–0.90
	100–160	1.67–4.98
Fe^{4+}	60–80	0.13–0.27
	80–140	0.49–1.87
Fe^{5+}	70–150	0.35–2.25
Fe^{6+}	100–160	1.67–4.98

The results of these measurements are shown as black curves on Fig. 1 for Fe^{2+} to Fe^{6+} ions from top to bottom, respectively. They correspond to the variation as a function of photon energy of the absolute single photoionization cross sections. Each curve results from the average of several scans recorded during two different beam-time periods. The gray vertical error bars on the figure give the statistical uncertainty on each data points. The variation in the amplitude of the error bars observed on each spectrum as a function of photon energy is due to a large extent to the variation in the photon flux with photon energy. The magnitude of the cross section displayed here for Fe^{4+} ion is close to the one previously published [12] but with a statistical uncertainty im-

proved by more than a factor of 2. The difference arises from a wrong determination of the uncertainty in the previously published data.

The systematic uncertainty on the measured cross sections is usually between 10% and 15%, and is mainly due to the uncertainty on the beam overlap and photon flux determinations [21]. It is higher, of the order of 20%, for the present determination of Fe^{2+} and Fe^{4+} cross sections because of contamination of the incident ion beam by ions with the same mass to charge ratio not separated by the first dipole magnet, namely, N_2^+ and CO^+ for Fe^{2+} ion and N^+ for Fe^{4+} ion. In the case of Fe^{4+} ion, it was possible to estimate the percentage of the contaminant because the photoionization cross section for N^+ ion was previously measured [12]. The same procedure cannot be applied in the case of Fe^{2+} ions since two contaminants can contribute. The relative population of $^{56}Fe^{2+}$ ion in the incident ion beam was estimated from the intensity of the expected nonpolluted $^{54}Fe^{2+}$ isotope peak observed in the mass spectra recorded before and after each photon energy scan using the first dipole magnet. The relative population of ^{54}Fe isotope in the natural iron (6.37%) was taken from Ref. [23]. Below 35 eV, the cross sections are not reliable as they can be affected by higher-order contribution.

It is well known that ECRIS produces ions in ground and excited states. All the excited states with decaying lifetime longer than the time of flight of the ions between the source and the interaction region (typically a few microseconds) can contribute to the recorded spectra. Concerning the Fe^{Q+} ions with $Q=2-6$, this is the case for all the excited states having the same configuration as the ground state, namely, $Fe^{Q+}\ 3p^6 3d^{(8-Q)}$. The states of the first-excited configuration, namely, $Fe^{Q+}\ 3p^6 3d^{(7-Q)}4s^1$, have the same parity as the ground state, and ions in these excited states can also be present in the interaction region. The position of the ionization threshold for each term with the same configuration as the ground state are shown on Fig. 1 as the black vertical bars above the cross section for each charge state [24]. The position of the threshold for ions in the ground state corresponds to the bar at the highest energy. For all charge state, the rise of the signal appears in the same energy range as these thresholds, showing that the ionic targets are composed of ions in the different states with the same configuration as the ground state. In opposite, no clear signal is observed below, indicating that there is no important contribution of the higher excited states with one electron in the $4s$ orbital. This point will be discussed further during the discussion on the Opacity Project results.

After the onset of the cross sections at the thresholds, prominent $3p \rightarrow 3d$ UTAs are observed for the lower charge states above the slowly decreasing continuous signal due to direct photoionization process. The energy of the UTA is slowly increasing and they are broadening with increasing charge state (the barycenter of the structure is at 56.0 eV for neutral Fe [25], 57.9 eV for Fe^+ [11], 60.6 eV for Fe^{2+}, and 64.6 eV for Fe^{3+}). As their position shifts more slowly than the position of the ionization thresholds, a crossing occurs for Fe^{4+} ion. All the transitions of the UTA lying below the thresholds decay via fluorescence and cannot be observed here. In the case of Fe^{5+} and Fe^{6+} ions, all $3p \rightarrow 3d$ transitions are at lower energy than the thresholds, and the observed structures correspond mainly to the $3p \rightarrow 4d$ excitations.

It was possible to measure the double photoionization cross section in the case of the Fe^{3+} incident ion only. It is shown on the inset in the second panel starting from the top. In the case of Fe^{2+} ion, a too low signal-to-noise ratio prevented us from observing the double-ionization signal. For Fe^{4+} ions and higher charge states, thresholds for double ionization are already higher than the maximum energy range considered here.

III. OPAS CODE

We have performed calculations using a spectral opacity code (OPAS). For each ionic state, the total photoionization cross section is evaluated as a sum of direct and resonant contributions from all the levels of the ground configuration. The direct photoionization cross sections from $3d$, $3p$, and $3s$ subshells are evaluated from one-electron calculations using the length form of the electric-dipole operator. The radial functions for bound electrons are obtained from the minimization of the ground configuration energy using the optimized potential method [26]. The radial functions for free electrons are calculated in the same optimized potential. The energy thresholds are evaluated from the initial and final configuration average energies independently minimized, and a statistical relativistic energy shift is included. The edges are dressed using a profile taking into account the initial and final configuration energy variances. The resonant photoexcitation cross sections involving $3p \rightarrow ns, nd$ transitions have been considered. The calculations were limited here to principal quantum number up to 6. For each pair of configurations connected by an electric-dipole transition, the calculation of the individual lines, based on a full intermediate coupling in the jj basis, is performed using a MCDF code [27]. The Babushkin gauge, which corresponds to the length form in a nonrelativistic calculation, is used. In order to preserve the f-sum rule, the total oscillator strength is normalized to the one deduced from the one-electron calculation using bound radial functions computed in the optimized potential mentioned above. Once again, the length form of the electric-dipole operator is used. Then, only photoexcited levels above the first ionization limit were retained, and a statistical population of the initial levels was assumed. A Lorentzian profile was used for each line shape with a full width at half maximum (FWHM) equal to the natural width which is dominated here by autoionization processes. The autoionization rates are evaluated using bound radial functions computed in the optimized potential of the photoexcited configurations. The resulting spectrum was then convoluted with a Gaussian function with variable FWHM as indicated in Table I to account for the finite spectral resolution.

The results are shown as gray curves on Fig. 2, compared with the experimental cross sections (black curves). The experimental cross section given here (and in the following figures) for Fe^{3+} ion is the sum of the single and double photoionization cross sections shown separately on Fig. 1.

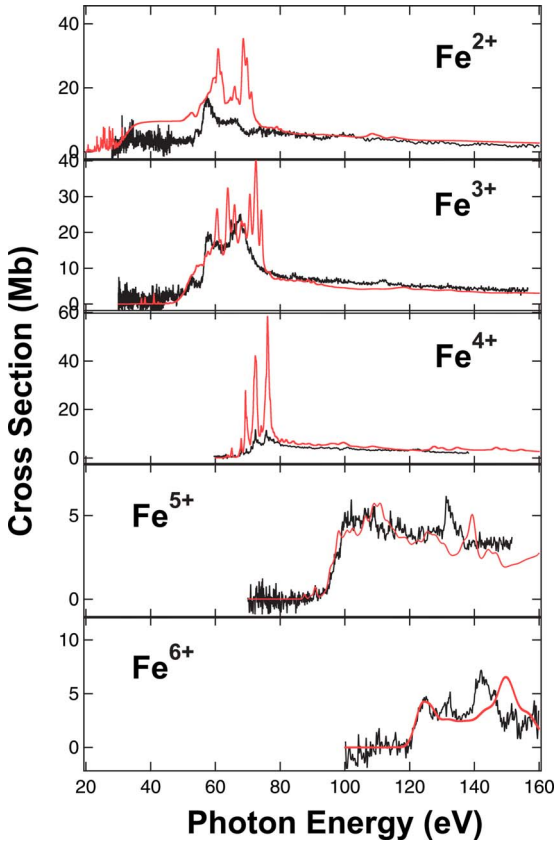

FIG. 2. (Color online) Comparison of the synthetic spectra (gray curves) reconstructed from the photoexcitation and photoionization cross sections we have calculated using the OPAS code (see text for details) with the experimental spectra (black curves). On this figure and the following, the experimental cross section for Fe^{3+} ion is obtained as the sum of single and double photoionization cross sections.

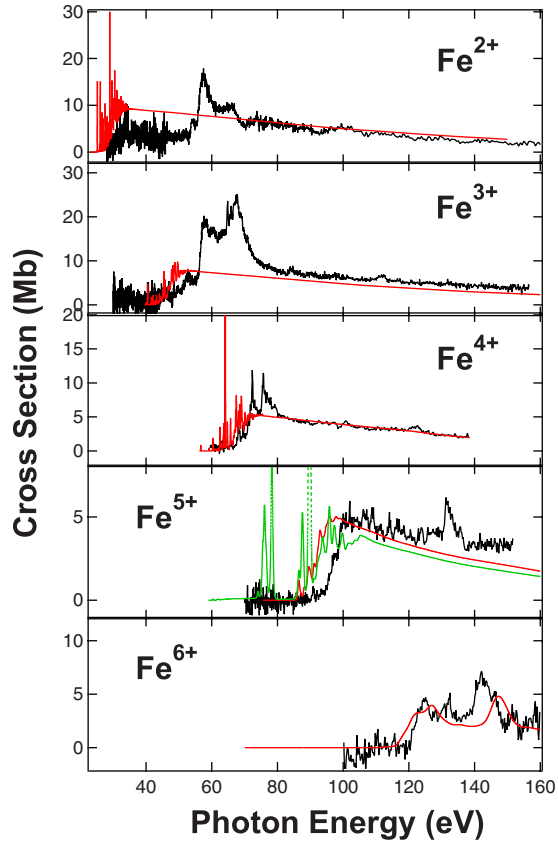

FIG. 3. (Color online) Comparison of the synthetic spectra (gray curves) reconstructed from the photoionization cross sections available in the TOPbase [38] (see text for details) with the experimental spectra (black curves). For Fe^{5+} ion, the dotted curve gives the synthetic spectrum constructed including the contribution of all the terms of the $3d^24s$ and $3d^3$ configurations.

Except for Fe^{2+} and Fe^{4+} ions, the overall agreement with experiment is satisfactory. In particular, the direct photoionization process is well described, within the experimental uncertainties, for all charge states in the high-energy region, and position of the ionization thresholds is in good agreement with previous determinations [24]. The position of the UTA is also well reproduced, but the calculations predict more structures than observed in the experimental spectra, indicating that the natural width of the transitions is underestimated. In contrast, our previous calculations for Fe^{4+} ion [12] were strongly overestimating the width. The difference arises from a wrong calculation of the autoionization rates in the previously published calculations. Three major discrepancies are noticeable. First, for Fe^{2+} ion, the calculated direct photoionization is too high by a factor of 3 in the 30–55 eV photon energy range. One explanation, at least in the 40–55 eV energy range, could be interference effects between the direct and resonant photoionization processes, effect which is not taken into account in the OPAS code. Indeed, such effect was previously observed in the photoionization cross section of Fe^{+} ion [11] and was well described by *R*-matrix calculations, taking into account this interference effect [28]. The second main difference lies in the photoionization cross section of Fe^{3+} in the 80–120 eV photon energy range, which is 30% lower in the calculations. Finally, the intensity of the UTA is overestimated in the calculations by a factor of 2 in the case of Fe^{2+} ion and a factor of 3 for Fe^{4+} ion. If there is no straight explanation for Fe^{2+} ion, in the case of Fe^{4+} ion it is worthwhile to emphasize the extreme sensitivity of the UTA calculated intensity to the calculated position of the overlapping thresholds [29]. Our calculations predict that only half of the intensity of the UTA lies above the thresholds. This intensity can be reduced by a factor of 2 if we arbitrarily increase the thresholds energy by 4 eV.

IV. COMPARISON WITH OTHER THEORIES

A. *R*-matrix calculations

A large number of *R*-matrix calculations have been performed to determine the photoionization cross sections of iron ions, resumed in at least nine publications only restricting to Fe^{2+} to Fe^{6+} ions [29–37]. The first calculations were performed in the frame of the Opacity Project and are available in the TOPbase [38]. Their results for Fe^{2+} to Fe^{6+} ions are displayed on Fig. 3 as the thin continuous gray lines in comparison with the experimental cross sections. These synthetic theoretical spectra have been obtained using the same

procedure as for the OPAS results by summation of the individual photoionization cross sections of each term with the same configuration as the ground state, weighted by their statistical weight. The resulting spectra were then convoluted with a Gaussian function with the variable FWHM given in Table I to account for the finite experimental bandpass. All the Opacity Project calculations have been performed in *LS* coupling, and because the preliminary goal of this large international collaboration was to provide an extended number of photoionization cross sections for all the ions of the astrophysical abundant elements (of atomic number $Z \leq 26$) in the ground state and many excited states, only the discrete photoexcitation of the most outer electron was in general considered. Then the UTA structures, involving excitation of a $3p$ inner-shell electron, are not reproduced, resulting in a large underestimate of the cross sections by up to a factor 4 in the energy range of the UTA. The $3p \rightarrow 3d$ excitations were included in the case of Fe^{6+} ion [31]. A systematic shift of the ionization thresholds toward the low photon energies is observed for all charge states, up to 5 eV for the lower charge states. At higher photon energy, the direct photoionization cross sections are well described except for an underestimate of the cross section for Fe^{3+} ion. Let us note also that for Fe^{2+} ion, as predicted by the OPAS calculations, the calculated cross section is twice higher than the experimental one in the energy range 30–50 eV.

In order to investigate the effect of a possible contribution of ions in excited states with one electron promoted to the $4s$ orbital for the experimental spectra, we have rebuilt a synthetic spectrum for Fe^{5+} ion including also the calculated photoionization cross sections for all the terms with $3d^2 4s$ configuration available in the TOPbase in addition to the $3d^3$ configuration, assuming a statistical population of all the terms. The result is given by the dotted curve on Fig. 3. Fe^{5+} ion was chosen because the experimental spectrum for this ion was recorded using the highest radio frequency power for heating of the ECRIS plasma (30 W), giving the most favorable conditions for excited states production. Our synthetic spectrum predicts very strong lines, in particular around 78 and 89.5 eV, which are not observed in the experimental spectrum, strengthening our assumption that mainly excited states with the same configuration as the ground state contribute significantly to the experimental spectra.

Results of more recent *R*-matrix calculations, performed as an extension of the Opacity and Iron Projects for Fe^{2+} [32], Fe^{3+} [35], and Fe^{4+} [29,36] ions, are displayed as gray curves in Fig. 4, from top to bottom, respectively (data from Refs. [32,35,36] are available at websites given in Ref. [43]). The same procedure as for OPAS and TOPbase results was applied to reconstruct the synthesized theoretical spectra; they are obtained from the weighted sum of the cross sections for all terms with the same configuration as the ground state and then convoluted with a Gaussian function with variable FWHM. The Fe^{2+} calculations were performed using an extended eigenfunction expansion (49 states against 16 for the TOPbase data [30]) but not including the $3p \rightarrow 3d$ excitations. Despite the extended base, the agreement of these *R*-matrix results with the experimental spectrum appears to be worse than the one achieved by the TOPbase calculations, especially in the high-energy region where the cross section

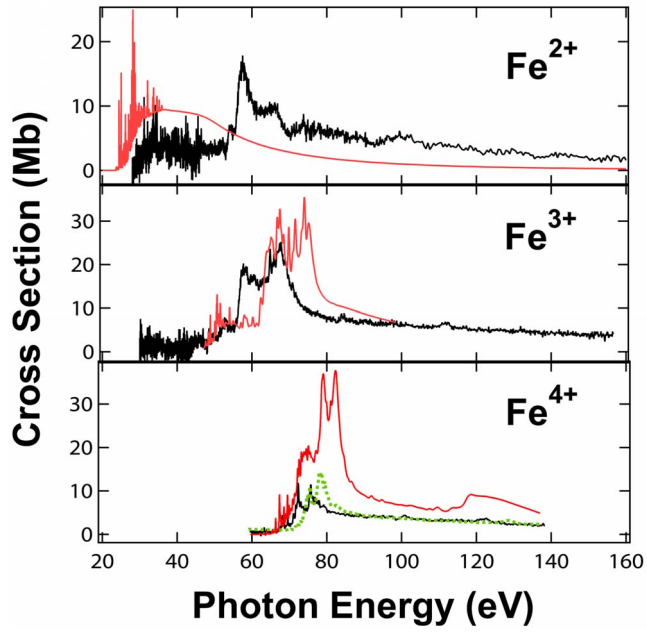

FIG. 4. (Color online) Comparison of the synthetic spectra (gray continuous curves) reconstructed from the photoionization cross sections obtained from *R*-matrix calculations for Fe^{2+} [32], Fe^{3+} [35], and Fe^{4+} [36] ions (see text for details) with the experimental spectra (black curves). For Fe^{4+} ion, the dotted curve gives the synthetic spectrum constructed from the most recent *R*-matrix calculations [29].

for the direct photoionization process is strongly underestimated. The $3p \rightarrow 3d$ inner-shell excitations are included in the Fe^{3+} and Fe^{4+} calculations. For the first one, the width of the UTA is rather well reproduced but with more pronounced structures than observed on the experimental spectrum, in the same way as the OPAS results. The intensity is slightly overestimated, and the position is too high by 5 eV compared to the UTA position. For Fe^{4+} ion, the 39 term eigenfunction expansion [36], shown as continuous gray curve on the bottom panel of Fig. 4, totally failed to correctly reproduce the UTA and the direct photoionization intensity. In opposite, the most recent calculations by Bautista [29] achieved a very good agreement with the experiment, performing a careful analysis of the important effects to include in the calculations, namely, (1) the one-electron orbital used to represent the target ion must be optimized on the target itself and on the states of the ionizing system as well in order to obtain a good position of the UTA; (2) the parent states $3p^5 3d^{N-1}$ must be included to account for the coupling of the $3p^5 3d^N$ states with the continuum; (3) unresolved narrow and high resonances, which can create unphysical troughs in the synthetic spectra, must be carefully eliminated. The principal remaining difference between these calculations and the experimental cross section is a shift of 3 eV of the UTA toward high photon energies.

Finally, Fig. 5 shows the results of relativistic *R*-matrix calculations, including inner-shell photoionization processes down to the K shell and, of particular here, the effects of $3p \rightarrow 3d$ excitations [37]. Only the ground state of each ion is

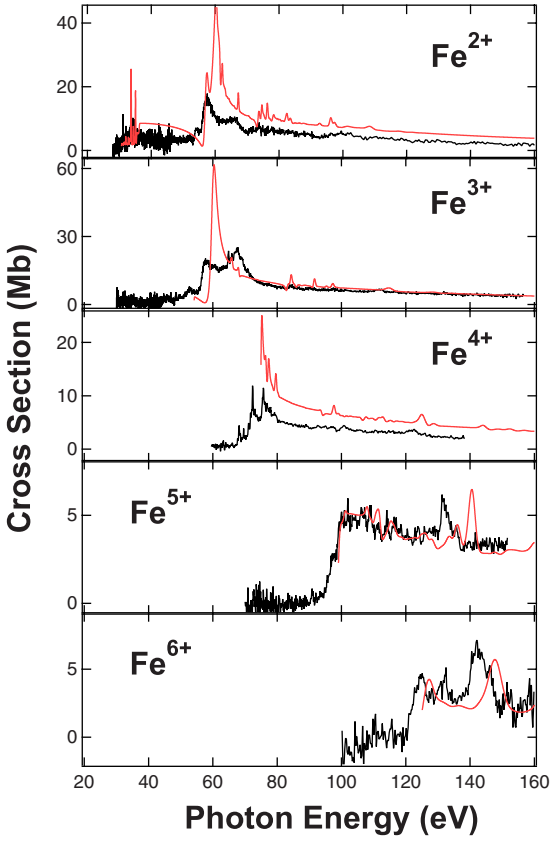

FIG. 5. (Color online) Comparison of the synthetic spectra (gray curves) reconstructed from the photoionization cross sections obtained from the *R*-matrix calculations of Berrington and Ballance [37] with the experimental spectra (black curves).

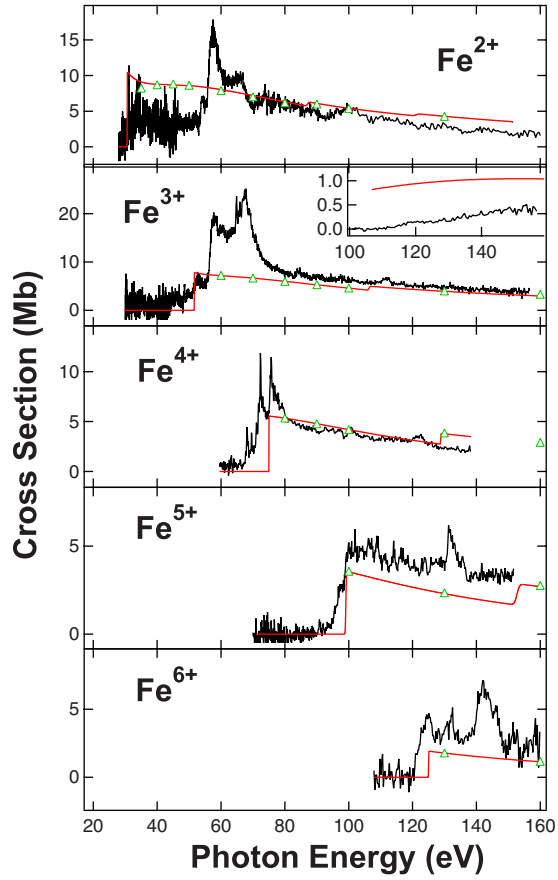

FIG. 6. (Color online) Comparison of the photoionization cross sections calculated in the one-electron approximation (gray curves: Ref. [39]; open triangles: Ref. [40]) with the experimental spectra (black curves).

considered here in the initial state of the process. This restriction is expected to have small effect on the intensity of the direct photoionization cross sections which is independent, within a similar configuration and neglecting electron correlations, of the term of the initial state. In opposite, it will reduce strongly the number of resonances and then the width of the UTA. The calculated cross sections have been convoluted with the Gaussian function of variable FWHM as before. Agreement between these results and the experiment is quite good for Fe^{5+} and Fe^{6+} ions, as well as for the Fe^{3+} direct photoionization process. The position of the UTA is also well reproduced but, as expected, their width is underestimated. There is still a marked difference in the case of Fe^{4+} ion, which probably can be accounted for an overestimate of the direct photoionization cross section. Let us note that, for Fe^{2+} ion, these calculations predict indeed the interference effect between the resonant and the direct photoionization channels below the UTA as discussed previously but on a too narrow energy range to reproduce correctly the experimental cross section down to the threshold.

B. Central field approximations

For many practical applications, the use of photoionization cross sections free of any resonant structures is considered as very convenient. Several approaches have been proposed, including direct photoionization cross-section calculations in the central field approximation [39,40] or averaging over the resonances of the Opacity Project cross sections [41,42]. This second set of data being based on the TOPbase data already discussed will not be considered further here. Figure 6 presents the results of the central field calculations, compared to the experimental cross sections. The Hartree-Dirac-Slater (HDS) values, interpolated using an analytical fit [39], are given by the gray curves and the Hartree-Slater values [40] are given by the open triangles. The two calculations differ mainly by the inclusion of relativistic effects, expected not to play an important role for the light ions and the low-energy range considered here. Then it is not a surprise that they give almost similar results. Only ions in the ground configuration have been considered in the initial state of the photoionization process in both calculations. Upon the photoionization cross sections in the $3d$ subshell, steps are predicted by the calculated cross sections at the aperture of the $3p \rightarrow \varepsilon s, \varepsilon d$ channels (and the $3s \rightarrow \varepsilon p$ channel at 121.1 eV for Fe^{3+} ion). Except for the first threshold, they are not observed experimentally. Several Rydberg series converge to inner-shell thresholds, blurring the transition between resonant photoionization below threshold and direct photoionization above. Except for the Fe^{2+} and Fe^{5+} ions, the $3d$ experimental cross section is well reproduced at

photon energy below the aperture of the $3p \rightarrow \varepsilon l$ channels.

Two processes can contribute to the intensity of the double-ionization cross section: direct double photoionization (shake off) and Auger decay of the $3p^{-1}$ hole when it is energetically allowed. Usually, the shake off cross sections are weaker by several orders of magnitude than the $3p$ photoionization cross section, especially at photon energies close to the double-ionization threshold. The experimental double-ionization cross section for Fe^{3+} is shown in the inset of Fig. 6, together with the results of the HDS calculations for photoionization in the $3p$ subshell. The calculated cross section is by far the highest. The calculated threshold for photoionization in the $3p$ subshell is 106.7 eV, 10 eV below the lowest double-ionization threshold [24]. The weak intensity of the experimental cross section confirms that the Auger decay of the $3p^{-1}$ hole is not allowed and only the shake off contributes to the signal close to threshold. As the photon energy increases, the Auger decay of $3p \rightarrow \varepsilon l$ satellite channels, involving in addition the simultaneous excitation of one outer electron to an empty orbital, becomes allowed and explains the increase in the experimental double photoionization cross section.

V. CONCLUSION

Absolute photoionization cross sections of Fe^{2+} to Fe^{6+} ions have been measured over an extended photon energy range, from the first ionization threshold up to 160 eV. Cross sections for single photoionization, as well as for double ionization in the case of Fe^{3+} ion, have been obtained. These measurements were compared with the results of the calculations we performed using the OPAS spectral opacity code, as well as with the results of *R*-matrix and one-electron calculations used for the determination of astrophysical plasmas opacity. Our results emphasize the necessity to include the $3p$ inner-shell excitation to correctly describe in this energy range the opacity of low-temperature plasmas in which iron ions with charge state lower than 5 have a strong contribution. Except for the most recent *R*-matrix calculations for Fe^{4+} ion, none of the theoretical results gives a satisfactory description on the $3p \rightarrow 3d$ UTA. Most of the time, the intensity of the UTA is strongly overestimated by the calculations.

To summarize these results, we have reported on Fig. 7 the oscillator strengths determined by integration of the spectra between 20 and 140 eV photon energy as a function of the ion charge state. The experimental values (black points) are compared with the results of OPAS (dashed line), TOPbase [38] (continuous line), Berrington and Ballance [37] *R*-matrix (dashed-dotted line), and one-electron [39] (dotted line) calculations. The continuous decreasing of the integrated oscillator strength with increasing charge state can be accounted to both the decrease in the number of electrons in the initial state and the shift of the first ionization threshold toward higher photon energy while less and less electrons become available for screening of the nucleus attractive potential. The reduction by a factor close to 3 observed experimentally between Fe^{3+} and Fe^{4+} results from the sliding of the $3p \rightarrow 3d$ UTA relative to ionization threshold. The UTA overlaps with the threshold in the case of Fe^{4+}, making this ion a very stringent test for the models. One unexplained observation is the low value measured for Fe^{2+} ions. Theoretical predictions can be divided into two groups. The ones which take into account the $3p \rightarrow 3d$ transitions (OPAS and Berrington and Balance [37] calculations) are in agreement with the measurement for Fe^{3+} ion but not for Fe^{4+} ion. Those which does not account for the $3p \rightarrow 3d$ transitions (TOPbase [38] and one-electron [39] calculations), expected to be the less accurate, are more in agreement with Fe^{2+} and Fe^{4+} experimental values. Other theoretical investigations are needed to explain this observation and to achieve a better description of the UTA for the low-charged iron ions. On the experimental side, addition of the contribution of double photoionization, not measured in the present investigation for Fe^{2+} ion, will increase the measured oscillator strength for this ion. A small contamination of the tiny $^{54}Fe^{2+}$ isotope peak, used as a reference for the determination of the density of the Fe^{2+} ionic target, could explain also an underestimate of the Fe^{2+} photoionization cross section over the whole photon energy range. Nevertheless, no significant difference is observed for this ion between the theoretical and the experimental cross sections in the high photon energy range. One way to check this possibility would be to repeat the Fe^{2+} measurements using pure ^{54}Fe isotope.

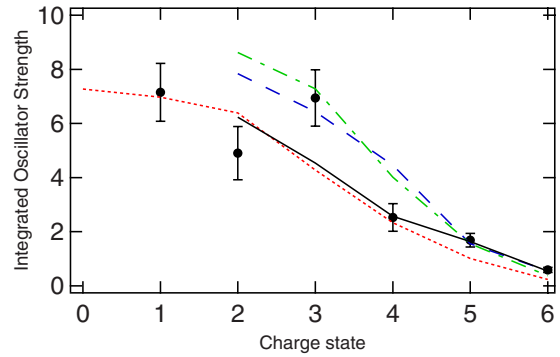

FIG. 7. (Color online) Variation in the oscillator strengths determined by integration of the spectra between 20 and 140 eV photon energy as a function of the ion charge state. The experimental values (black points) are compared to the results of OPAS (dashed line), TOPbase [38] (continuous line), Berrington and Ballance *R*-matrix [37] (dashed-dotted line), and one-electron [39] (dotted line) calculations. The experimental value for Fe^{+} is obtained from the data of Ref. [10].

ACKNOWLEDGMENTS

The authors would like to thank the support of the European Community—Research Infrastructure Action under FP6 Structuring the European Research program (IA-SFS) (Contract No. RII3-CT-2004-506008). They are also grateful to the ISA staff of the Aarhus University for their helpful assistance.

[1] M. A. Bautista and A. K. Pradhan, Astrophys. J. **492**, 650 (1998), and references therein.
[2] S. R. Becker and K. Butler, Astron. Astrophys. **265**, 647 (1992).
[3] M. Rodríguez and R. H. Rubin, Astrophys. J. **626**, 900 (2005).
[4] K. L. Bell, Phys. Scr. T **T100**, 64 (2002).
[5] T. R. Kallman and P. Palmeri, Rev. Mod. Phys. **79**, 79 (2007).
[6] S. Muto, S. Morita, and The LHD Experimental Group, J. Plasma Fusion Res. **3**, S1086 (2008).
[7] J. E. Bailey *et al.*, Phys. Rev. Lett. **99**, 265002 (2007).
[8] S. Johansson *et al.*, Phys. Scr. T **T100**, 71 (2002).
[9] J. B. West, J. Phys. B **34**, R45 (2001).
[10] H. Kjeldsen, J. Phys. B **39**, R325 (2006).
[11] H. Kjeldsen *et al.*, J. Phys. B **35**, 3655 (2002).
[12] J. M. Bizau, C. Blancard, D. Cubaynes, F. Folkmann, D. Kilbane, G. Faussurier, H. Luna, J. L. Lemaire, J. Blieck, and F. J. Wuilleumier, Phys. Rev. A **73**, 020707(R) (2006).
[13] D. J. Botto, J. McEnnan, and R. H. Pratt, Phys. Rev. A **18**, 580 (1978).
[14] R. F. Reilman and S. T. Manson, Astrophys. J., Suppl. **40**, 815 (1979).
[15] D. A. Verner *et al.*, At. Data Nucl. Data Tables **55**, 233 (1993).
[16] M. J. Seaton, J. Phys. B **20**, 6363 (1987); The Opacity Project Team, *The Opacity Project* (Institute of Physics, Bristol, 1995), Vol. 1.
[17] D. G. Hummer *et al.*, Astron. Astrophys. **279**, 298 (1993).
[18] K. A. Berrington and C. Ballance, J. Phys. B **34**, 2697 (2001).
[19] M. Martins *et al.*, J. Phys. B **39**, R79 (2006), and references therein.
[20] J. E. Hansen *et al.*, J. Phys. B **40**, 293 (2007).
[21] H. Kjeldsen *et al.*, Nucl. Instrum. Methods Phys. Res. B **234**, 349 (2005).
[22] R. Lang *et al.*, Rev. Sci. Instrum. **71**, 651 (2000).
[23] K. J. R. Rosman and P. D. P. Taylor, Isotopic Compositions of the Elements, 1997, available at http://physics.nist.gov/PhysRefData/Compositions/index.html
[24] Yu. Ralchenko, A. E. Kramida, J. Reader, and The NIST ASD Team, NIST Atomic Spectra Database (Version 3.1.5), National Institute of Standards and Technology, Gaithersburg, MD, 2008, http://physics.nist.gov/asd3
[25] H. Feist, M. Feldt, C. Gerth, M. Martins, P. Sladeczek, and P. Zimmermann, Phys. Rev. A **53**, 760 (1996).
[26] J. D. Talman and B. A. Shadwick, Phys. Rev. A **14**, 36 (1976).
[27] J. Bruneau, J. Phys. B **17**, 3009 (1984).
[28] K. A. Berrington and B. Ballance, J. Phys. B **34**, L383 (2001).
[29] M. A. Bautista, J. Phys. B **39**, L361 (2006).
[30] P. M. J. Sawey and K. A. Berrington, J. Phys. B **25**, 1451 (1992).
[31] H. E. Saraph, P. J. Storey, and K. T. Taylor, J. Phys. B **25**, 4409 (1992).
[32] S. N. Nahar, Phys. Rev. A **53**, 1545 (1996).
[33] M. A. Bautista, Astron. Astrophys. Suppl. Ser. **119**, 105 (1996).
[34] M. A. Bautista and K. A. Pradhan, Astron. Astrophys. Suppl. Ser. **126**, 365 (1997).
[35] S. N. Nahar, M. A. Bautista, and A. K. Pradhan, Phys. Rev. A **58**, 4593 (1998).
[36] S. N. Nahar and M. A. Bautista, Astrophys. J., Suppl. Ser. **120**, 327 (1999).
[37] K. A. Berrington and C. Ballance, J. Phys. B **34**, 2697 (2001).
[38] W. Cunto, C. Mendoza, F. Ochsenbein, and C. J. Zeippen, Astron. Astrophys. **275**, L5 (1993).
[39] D. A. Verner and D. G. Yakovlev, Astron. Astrophys. Suppl. Ser. **109**, 125 (1995).
[40] R. F. Reilman and S. T. Manson, Phys. Rev. A **18**, 2124 (1978).
[41] D. A. Verner *et al.*, Astrophys. J. **465**, 487 (1996).
[42] M. A. Bautista, P. Romano, and A. K. Pradhan, Astrophys. J., Suppl. Ser. **118**, 259 (1998).
[43] http://www.astronomy.ohio-state.edu/~nahar/nahar_radiativeatomicdata/index.html